NMR evidence for change in the local structure of $ZrCr_2H_x$

Ronald Dean Stoddard and Mark S. Conradi
Department of Physics, CB 1105, Washington University, One Brookings Drive, St. Louis, Missouri 63130
(Received 16 September 1997)

We report here measurements of $T_{1\rho}^{-1}$, the spin-lattice relaxation rate in the rotating frame, for protons from 4 to 300 K in two samples of $ZrCr_2H_x$, with $x=0.2$ and 0.5. We find, especially for $x=0.2$, that the maximum rate $(T_{1\rho}^{-1})_{MAX}$ is substantially larger than expected from the laboratory frame spin-lattice relaxation rate T_1^{-1} by comparison with a model that successfully fits the T_1^{-1} data. Further, a dimensionless parameter $\Re$ is formed that expresses the relative strength of $(T_1^{-1})_{MAX}$ after correction for the different measurement frequencies. The measured values of $\Re$ for $x=0.2$ are larger by a factor of 2 or more than that of any simple model, indicating that the dipolar second moment M_2 (primarily proton-proton) increases as temperature decreases, a surprising result. The increasing second moment is confirmed by direct measurement from dipolar echoes (magic echoes) at low temperature. The increased second moment reflects either decreasing average H-H distances below 150 K (partial clustering, a change in the local structure) or the progressive freeze-out of motional averaging of M_2 by high-frequency local motions. [S0163-1829(98)04417-8]

I. INTRODUCTION

Hydrides formed from Laves-phase metals (AB_2 compounds) have several useful characteristics for practical applications in hydrogen storage. First, many of the hydrides exhibit unusually high hydrogen mobility. Second, there are large single-phase regions of the T-x phase diagram. Finally, the hydrogen-vapor pressure can be tuned by choice of the metals A and B; for example, one or the other may be a nonhydriding or weakly hydriding metal.

The hydrogen-atom diffusion in Laves-phase metal hydrides is characterized by unusually small activation energies. For example, in the $C15$ structured form of $ZrCr_2H_x$ at low concentrations ($x \leqslant 0.5$), the hydrogen atoms move fast enough to completely motionally narrow the proton nuclear magnetic resonance (NMR) line shape at 80 K.[1,2] This indicates that the hydrogen atoms hop at a rate of at least 10^5 s^{-1} by 80 K.

Some of the Laves-phase hydrides also display hydrogen motion on two distinct time scales. This is most apparent in $C15$-TaV_2H_x, where two separate peaks are visible in the proton spin-lattice relaxation rate T_1^{-1}.[3] The high-temperature peak represents long-range diffusive motions, while the low-temperature peak is from a local motion. Quasielastic neutron-scattering measurements on this system confirm the coexistence of motion occurring on two time scales. The neutron data indicate that the local (more rapid) hydrogen motion involves jumping between three or six sites on a circle of radius ~ 1.1 Å.[4]

Another interesting aspect of Laves-phase metal hydrides is the ability to cross wide regions of the phase diagram without encountering a phase transition. An example of this is $C15$-ZrV_2H_x, where the hydrogen concentration can be continuously varied from $x=0$ to $x=6.0$ at room temperature without a phase transition.[5] A second example is $C15$-$ZrCr_2H_x$ ($x \leqslant 0.5$), where there is no evidence of a phase transition to an ordered hydride phase down to at least 11 K,[1,2] in agreement with the tentative phase diagram for $C15$-$ZrCr_2H_x$.[6]

The Laves-phase intermetallic compounds possess three different structures, the cubic $C15$ structure (space group $Fd3m$-O_h) and the hexagonal $C14$ and $C36$ structures (space group $P6_3/mmc$-D_{6h}^4) with four and eight AB_2 formula units per unit cell, respectively.[7] In the Laves phases all of the hydrogen interstitial sites are tetrahedral, with four metal-atom nearest neighbors. In the cubic structure there are 12 interstitials (g sites) with two A and two B nearest neighbors per AB_2 formula unit. In addition, there are four interstitials (e sites) with one A and three B nearest neighbors and one interstitial with four B nearest neighbors.[8] For $C15$-$ZrCr_2H_x$, only g sites are occupied[6,8] at low concentrations.

The purpose of this study is to better understand the unusual hydrogen motions in $C15$-$ZrCr_2H_x$ for low hydrogen concentrations ($x \leqslant 0.5$). While Skripov and co-workers observed that the proton NMR line in this system is completely motionally narrowed above 80 K, no study of the linewidth and line-shape changes has been made. In addition, they found that the T_1^{-1} relaxation peak (that occurs when the rate of atomic diffusion approximately matches the spin precession frequency) cannot be fit by a model for the motion with a single correlation time. Rather, a broad distribution of activation energies for the hydrogen motion was invoked resulting in a very broad distribution of correlation times. The origin of the distribution of activation energies in this crystalline solid solution is believed to be the disorder in the hydrogen positions. A model using the distribution was able to fit the T_1^{-1} data.[1] However, the second moments M_2 used to fit the data for $x=0.5$ and especially $x=0.2$ were considerably smaller than the Van Vleck calculated second moments[9,10] and, as we show here, smaller than the experimental results measured from essentially the free-induction decay (FID) at low temperatures.

Here we extend the NMR measurements to lower temperatures and frequencies by examining the relaxation rate in the rotating frame ($T_{1\rho}^{-1}$), pushing the relaxation peak to substantially lower temperatures. We find clear evidence that the

second moment in $C15$-$ZrCr_2H_x$ increases markedly as the temperature is reduced, particularly for the lowest concentration studied ($x=0.2$). The decrease in the second moment at high temperatures is due either to a gradual change in local structure or to rapid motional averaging in asymmetrical local potential wells.

II. EXPERIMENT

The $x=0.2$ and 0.5 samples used in this study were provided by Dr. Alexander Skripov of the Institute for Metals Physics in Ekaterinburg, Russia. These samples have been used in previous experiments;[1,11] details of the sample preparation are given in Ref. 1. The $C15$-$ZrCr_2H_x$ samples are not particularly air sensitive, but to prevent contamination sample handling was performed in a clean, nitrogen-filled glove bag. The $x=0.2$ and 0.5 samples were removed from the large Pyrex tubes used for shipping, placed into 6-mm-o.d. Pyrex tubes and sealed under $\frac{2}{3}$ atm of He gas for our measurements.

The NMR measurements detailed here were performed using a home-built, pulsed NMR spectrometer at frequencies of 21.3 and 5.3 MHz. The measurements were made in a home-built variable temperature Dewar. At low temperatures ($\leqslant$135 K), temperature regulation of the sample was accomplished by flowing temperature-controlled helium gas past the sample. At temperatures greater than 135 K, the NMR measurements were made as the temperature of the Dewar slowly equilibrated, either after the cryogens had been removed from the cold Dewar or after liquid nitrogen was added to the warm Dewar.

Temperature measurement was accomplished using a calibrated Lake Shore carbon-in-glass resistance thermometer placed in close proximity ($\sim$2 cm) to the sample. To provide an additional check, a type-T thermocouple (copper-Constantan) was also used.

The present studies concentrated on measurements of T_1 and $T_{1\rho}$. The T_1 measurements on the $x=0.2$ sample were made to ensure that the sample had not changed since the previous measurements.[1,11] The T_1 measurements used a saturation-recovery sequence.[12] Saturation was accomplished with a series of ten 90° pulses, with 1 ms between the pulses. The saturation train was followed by a waiting time τ during which the magnetization was allowed to recover. The magnetization was then measured from the FID following a single 90° inspection pulse. At least one value of τ was used that was long enough to allow the magnetization to return to essentially its equilibrium value $M(\infty)$. A plot of $[M(\infty)-M(\tau)]$ vs τ yielded an exponential decay. T_1 was taken as the point where the magnetization difference had decayed by $1/e$.

$T_{1\rho}$ measurements were made on both the $x=0.2$ and 0.5 samples with a standard spin-locking sequence.[12] The pulse sequence is initiated by a 90° pulse, which rotates the magnetization into the transverse plane. This is followed by a spin-locking pulse, 90° phase shifted with respect to the initial pulse. Thus, the spin magnetization is parallel to the effective field in the rotating frame. During the spin-locking pulse, the magnetization decays toward equilibrium (essentially zero) with the small rf field. After a time T the spin-locking pulse is shut off and the remaining magnetization is detected from the amplitude of the ensuing FID. For these measurements, a plot of $M(T)$ vs T yielded a decay that was nearly exponential. The relaxation rate $T_{1\rho}^{-1}$ was taken from the initial slope of the ln $M(T)$ vs T decay and thereby represents the *average* decay rate.

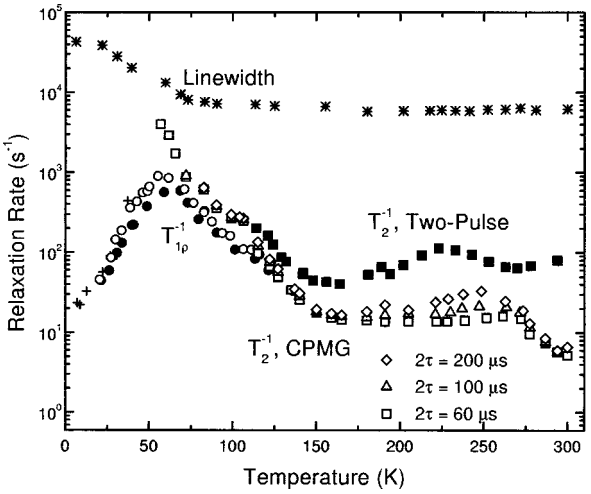

FIG. 1. Overview of data for $x=0.2$. The data shown are the NMR linewidth (stars), T_2^{-1} measured using both the two-pulse spin-echo (closed squares) and CPMG sequences. The CPMG measurements were made with three different values for 2τ, the spacing between π pulses. In addition, $T_{1\rho}^{-1}$ data were taken using two different rf field strengths, 22.7 kHz (open circles) and 39.1 kHz (closed circles), as well as T_{1D}^{-1} data (crosses). All of the data shown were obtained at an NMR frequency of 21.3 MHz.

In addition to the relaxation-rate measurements, the second moment M_2 (Ref. 10) of the samples was measured at temperatures low enough that all motion was essentially frozen out on the NMR time scale (the rigid lattice limit, 6.4 K for $x=0.2$ and 21.2 K for $x=0.5$). The M_2 measurements were made using a modification of the magic-echo sequence of Bowman and Rhim[13] that replaces the single preparation pulse of length $2t_d$ by two pulses of length t_d that are phase shifted by 180°. This modification of the magic-echo sequence compensates for rf-field inhomogeneities. The magic echo refocuses like-spin dipolar dephasing, displacing the echo peak to later times, away from the receiver blocking. Using several different values for t_d between 20 and 60 μs, the second moment was measured from the curvature of the refocused free-induction decay at the magic-echo peak. To confirm the time-domain results, the second moment was also determined by integration, using the real part of the Fourier transform of the time-domain signal. The two methods agreed as expected. M_2 showed no dependence on the value of t_d used in the measurement.

III. RESULTS AND DISCUSSION

An overview of the relaxation data for the $x=0.2$ sample is shown in Fig. 1. All of the data shown were obtained at an NMR frequency of 21.3 MHz. The data include measurements of the NMR linewidth T_2^{-1} (using both the Carr-Purcell-Meiboom-Gill, or CPMG, and two pulse spin-echo sequences[12]), $T_{1\rho}^{-1}$ at two rf field strengths, and T_{1D}^{-1} (the relaxation rate of the dipolar-ordered state, using the Jeener-

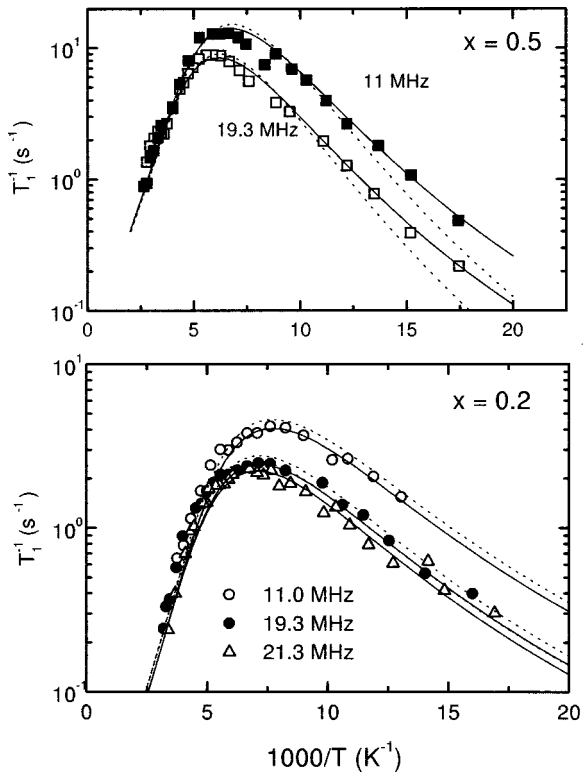

FIG. 2. T_1^{-1} data for $x=0.5$ and $x=0.2$ samples. All data for the $x=0.5$ sample are from Ref. 1, while the data for the $x=0.2$ sample are from Ref. 1 (11.0 and 19.3 MHz) and the present work (21.3 MHz). The solid curves represent our best fit to the T_1^{-1} data using a model with a Gaussian distribution of activation energies for the hydrogen motion; the dashed curves use the parameters of Ref. 1.

Broekaert sequence.[14]) Although we are primarily interested in T_1^{-1} and $T_{1\rho}^{-1}$ here, the additional data are presented as background. The T_2^{-1} data show an unusual second peak at higher temperatures, which is also seen in samples with hydrogen concentrations of $x=0.3$ and 0.5 (data not shown). The origin of this peak may be magnetic impurities in the $ZrCr_2$ host-metal lattice. The measured T_2^{-1} also shows a dependence on 2τ (the spacing between the rf π pulses) in the vicinity of the high-temperature peak. The 2τ dependence is characteristic of diffusion through a magnetic-field gradient and indicates that the frequency of the spins is changing on the time scale of 2τ (60–200 μs).

The NMR linewidth data demonstrate the extremely rapid hydrogen motion in the $x=0.2$ sample. The line narrowing begins at ~25 K, indicating that the hydrogen hopping rate at this temperature is of the order of the NMR linewidth,[15] 4×10^4 s^{-1}. In addition, the onset of motional narrowing is not very sharp. This may be due to local motions that only partially average the dipole-dipole interaction, or it may be due to a distribution of activation energies for the hydrogen motion. The samples with $x=0.3$ and 0.5 show similar behavior (not shown), but the onset of motional narrowing is shifted to higher temperature for both samples, indicating that the hydrogen motion is slower than for $x=0.2$.

Figure 2 presents T_1^{-1} for samples with hydrogen concentrations of $x=0.2$ and 0.5, respectively. All of the T_1^{-1} data are from Ref. 1, except for the 21.3-MHz measurements for $x=0.2$. The T_1^{-1} data for $x=0.2$ and 0.5 have been corrected to remove the electronic (Korringa) contribution to the relaxation,[1,15] leaving only the motional contribution. According to the theory of Bloembergen, Purcell, and Pound (BPP),[16] the motional contribution to T_1^{-1} is driven by fluctuations in the local fields caused by atomic motions. For hydrogen motion in $ZrCr_2H_x$, the fluctuations in local fields are due to motional modulation of the proton-proton dipole interaction (the metal nuclei have at most very small nuclear magnetic moments). For a powder sample, T_1^{-1} is given by[17]

$$T_1^{-1}=\left(\frac{4M_2}{3\omega_0}\right)\left(\frac{y}{4+y^2}+\frac{y}{1+y^2}\right), \tag{1}$$

where M_2 is the rigid lattice second moment and $y=\omega_0\tau_d$ (ω_0 is the NMR precession frequency and τ_d is the correlation time for the hydrogen motion). In many cases, τ_d obeys the Arrhenius relation

$$\tau_d=\tau_d(0)\exp\left(\frac{E_a}{k_BT}\right), \tag{2}$$

where E_a is the activation energy, k_B is the Boltzmann constant, and T is the absolute temperature. When the motion can be described using a single activation energy, Eq. (2) gives a single value for the correlation time at each temperature. Attempts to fit the T_1^{-1} data of Fig. 2 with a model employing a single activation energy are extremely unsuccessful (note the very different magnitudes of the slopes above and below the peaks in Fig. 2).

In Ref. 1 the T_1^{-1} data are successfully fitted with a model employing a Gaussian distribution of activation energies for the motion. The distribution of activation energies leads to a distribution of correlation times and the observed T_1^{-1} is a weighted sum of T_1^{-1} for each activation energy:

$$T_1^{-1}=\int_0^\infty T_1^{-1}(E_a)G(E_a)d(E_a), \tag{3}$$

where $G(E_a)$ is the Gaussian function describing the distribution of activation energies and $T_1^{-1}(E_a)$ is given by Eqs. (1) and (2). The fits with the parameters of Ref. 1 are shown in Fig. 2 as dashed curves. The solid lines in Fig. 2 represent our best fits with a Gaussian $G(E_a)$. Both sets of parameters are listed in Table I; the differences between the two sets are small.

Figure 3 shows rotating frame relaxation rate $T_{1\rho}^{-1}$ data for the same $x=0.2$ and 0.5 samples used in the T_1^{-1} experiments. For $T_{1\rho}^{-1}$, the electronic contribution to the relaxation is small enough that it can be neglected. The relation between the relaxation rate $T_{1\rho}^{-1}$ and fluctuations in the dipole-dipole interaction has been derived by Look and Lowe.[18] For a powdered sample, $T_{1\rho}^{-1}$ can be written[17]

$$T_{1\rho}^{-1}=\frac{M_2}{6\omega_0}\left(\frac{3y}{1+\omega_1^2\tau_d^2}+\frac{20y}{4+y^2}+\frac{2y}{1+y^2}\right), \tag{4}$$

where ω_1 is the strength of the rf field in angular frequency units. At our conditions, the first of the three terms above dominates. For a distribution of activation energies, $T_{1\rho}^{-1}$ is given by a weighted sum of $T_{1\rho}^{-1}$ for each activation energy:

TABLE I. Parameters used in fitting the T_1^{-1} data. Parameters were taken from Ref. 1 and this study.

	M_2 (s^{-2})	$\overline{E_a}$ (meV)	ΔE_a (meV)[a]	$\tau_d(0)$ (s)
$x=0.2$ (Ref. 1)	0.68×10^9	81	28	0.70×10^{-11}
$x=0.2$ (this study)	0.60×10^9	81	28	0.70×10^{-11}
$x=0.5$ (Ref. 1)	1.7×10^9	84	21	1.80×10^{-11}
$x=0.5$ (this study)	1.7×10^9	84	24	1.80×10^{-11}

[a]Refers to halfwidth at $\frac{1}{2}$ of maximum.

$$T_{1\rho}^{-1}=\int_0^\infty T_{1\rho}^{-1}(E_a)G(E_a)d(E_a). \tag{5}$$

Using this relation for $T_{1\rho}^{-1}$, we attempted to fit the $T_{1\rho}^{-1}$ data with the same parameters used to fit the T_1^{-1} data at higher temperatures. The dotted curves in Fig. 3 use the parameters of Ref. 1, determined from the T_1^{-1} data, while the solid lines use the parameters determined from our best fit of T_1^{-1}. The figure clearly shows that $T_{1\rho}^{-1}$ is not well described by either set of parameters with a Gaussian distribution of activation energies. In particular, the maximum $T_{1\rho}^{-1}$ relaxation rate for the $x=0.2$ sample is larger by a factor of ~3 than the models' prediction.

The large discrepancy between the measured and predicted maximum rates $T_{1\rho}^{-1}$ shows that no small adjustment of the parameters will allow the T_1^{-1} and $T_{1\rho}^{-1}$ data to be fit simultaneously. To further demonstrate this we have defined a dimensionless number $\Re$ such that

$$\Re\equiv\frac{(T_{1\rho}^{-1})_{\rm MAX}/(T_1^{-1})_{\rm MAX}}{\omega_0/\omega_1}. \tag{6}$$

$\Re$ expresses the strength of the maximum $T_{1\rho}^{-1}$ relaxation rate relative to the maximum T_1^{-1} relaxation rate, corrected for the different frequencies of the two measurements. For the BPP model, T_1^{-1} [Eq. (1)] reaches a maximum of

$$(T_1^{-1})_{\rm MAX}=(0.95)\,\frac{M_2}{\omega_0} \tag{7}$$

when $y=1.24$. Similarly, $T_{1\rho}^{-1}$ [Eq. (4)] reaches a maximum of

$$(T_{1\rho}^{-1})_{\rm MAX}=(0.25)\,\frac{M_2}{\omega_1} \tag{8}$$

when $\omega_1\tau_d=1$. Using these values for the maximum relaxation rates and Eq. (6), we obtain a value of $\Re=0.263$ for the BPP model. For a Gaussian distribution of activation energies, the maximum relaxation rates are suppressed by the spread in correlation times. The lower-frequency $T_{1\rho}^{-1}$ peak is suppressed more than the higher-frequency T_1^{-1} peak, because a given spread of activation energies generates a larger distribution of rates (when measured on a logarithmic scale) at low temperatures than at high. This argument is presented graphically in Fig. 4, an idealized relaxation map. The result

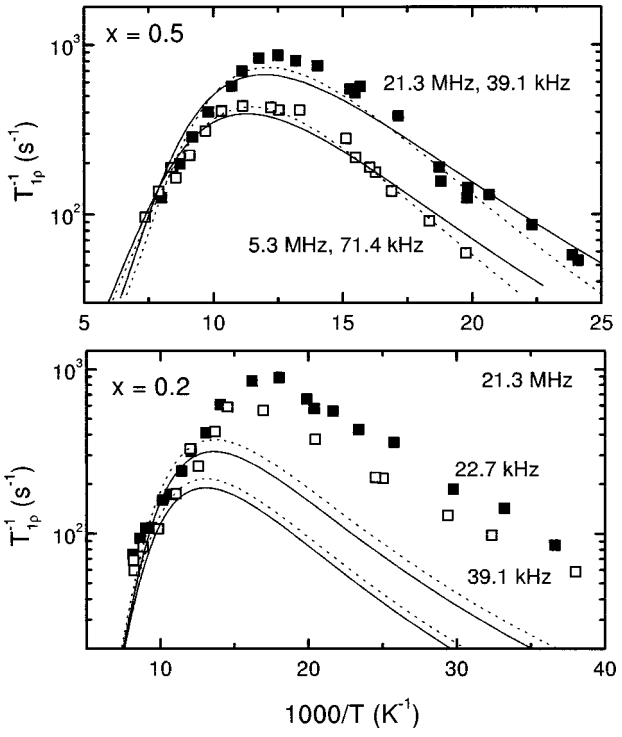

FIG. 3. $T_{1\rho}^{-1}$ data for the $x=0.5$ and $x=0.2$ samples. The data were taken at the NMR frequencies and nutation frequencies listed. The curves represent fits to the data using a model with a Gaussian distribution of activation energies for the hydrogen motion. The dashed curves represent fits to the data using parameters from Ref. 1, while the solid curves represent our best fits to the T_1^{-1} data of Fig. 2. The maximum $T_{1\rho}^{-1}$ rates are larger than the predictions of the models, especially for $x=0.2$. This demonstrates that the effective second moment of the spin-spin interactions increases with decreasing temperature.

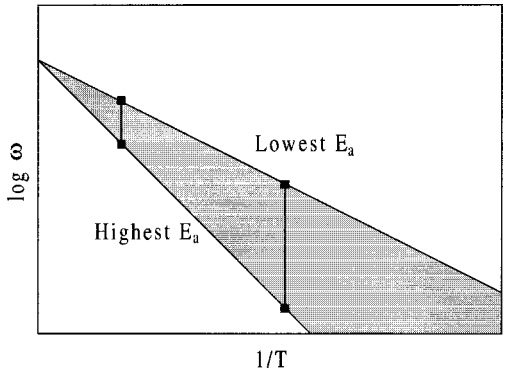

FIG. 4. Relaxation map showing a distribution of activation energies, represented by shaded region. At lower temperatures, the ratio of the highest rate to the lowest rate is larger than at high temperatures, as indicated by the lengths of the vertical bars. Thus, a distribution of activation energies is expected to decrease the maximum $T_{1\rho}^{-1}$ by a larger factor than the maximum T_1^{-1} is decreased.

TABLE II. $T_{1\rho}^{-1}$ and T_1^{-1} maxima at each frequency for $x=0.5$ as well as the calculated values for the parameter $\mathfrak{R}$.

$(T_{1\rho}^{-1})_{\mathrm{MAX}}$ (s^{-1})	Frequency (kHz)	$(T_1^{-1})_{\mathrm{MAX}}$ (s^{-1})	Frequency (MHz)	$\mathfrak{R}_{\mathrm{expt}}$	$\mathfrak{R}_{\mathrm{dist}}$[a]
862	39.1	12.7	11.0	0.241	0.168
862	39.1	8.85	19.3	0.197	0.160
435	71.4	12.7	11.0	0.222	0.180
435	71.4	8.85	19.3	0.182	0.171

[a]Calculated from Gaussian distribution of activation energies; see Table I, fourth row.

is a value for $\mathfrak{R}$ that is lower than the BPP value. We stress that a distribution of activation energies will always decrease $\mathfrak{R}$, regardless of the shape of the distribution. Table II shows the $\mathfrak{R}$ values calculated from each set of relaxation maxima for the $x=0.5$ sample; Table III shows the data for the $x=0.2$ sample. The values of $\mathfrak{R}$ for the $x=0.5$ sample are larger than expected for a Gaussian distribution of activation energies. In fact, the values for $\mathfrak{R}$ approach the BPP value of 0.263. The effect is much larger and is even striking for the $x=0.2$ sample, where the value of $\mathfrak{R}$ is considerably larger than the BPP value in all cases. This shows clearly that a model employing a distribution of activation energies absolutely cannot be used to simultaneously fit the T_1^{-1} and $T_{1\rho}^{-1}$ data, regardless of how one ''tunes'' the parameters of the distribution.

The above arguments demonstrate that no model with a *temperature-independent second moment* (assumption implicit in all the above models) is satisfactory. The simplest explanation for the increasing relaxation strength at lower temperatures is that M_2 grows as the temperature decreases. We remark that this is an unusual situation in the NMR study of solids. Generally, the only effect of temperature is to change the rate of the motions, as in Eq. (2).

Further evidence for the increase in the second moment with decreasing temperature is found in Table IV. There, second moments may be compared; the values are from fits to T_1^{-1}, fits to $T_{1\rho}^{-1}$, a Van Vleck rigid-lattice calculation,[1,10] and direct measurement by the magic-echo pulse sequence. For $x=0.2$, the second moments measured at decreasing temperatures (in the order T_1^{-1} fit, $T_{1\rho}^{-1}$ fit, and magic echo; corresponding to approximately 140, 60, and 6.4 K) form a clear progression to higher values. For $x=0.5$, this trend is present but much weaker. The data in Table IV confirm the conclusion that M_2 increases with decreasing temperature.

For $x=0.2$, the second moment that best fits the $T_{1\rho}^{-1}$ data is 33% larger than the M_2 from the T_1^{-1} fit. To fit the $T_{1\rho}^{-1}$ data, however, a substantially narrower distribution of activation energies is required ($\overline{E_a}=30$ meV and $\Delta E_a=8$ meV; compare with Table I). The narrower distribution and the increased M_2 both result in a substantial increase in the predicted maximum $T_{1\rho}^{-1}$ rate.

We believe that the increase in the second moment with decreasing temperature is due to a change in the *local* hydrogen structure. Although the exact nature of this change in $C15$-$ZrCr_2H_x$ is not known, such changes are observed in the rare-earth hcp solid solutions (ScH_x, LuH_x, and YH_x). Like $ZrCr_2H_x$, the hcp systems show no evidence of a transition to an ordered phase down to very low temperatures. Instead, the hcp solid solutions display a continuous change in the local hydrogen structure as the temperature is lowered. At low temperatures, the hydrogen atoms form pairs in second-nearest-neighbor sites, separated by metal atoms.[19–21] The hydrogen pairs form long, zigzag chains along the c direction of the host-metal lattice. As the temperature decreases, the number of hydrogen atoms participating in the pairing increases. Some form of hydrogen ordering in $C15$-$ZrCr_2H_x$ is expected at low temperatures for thermodynamic reasons. Specifically, the third law predicts a zero-entropy structure at zero temperature if the kinetics of the ordering process permit. While complete, long-range ordering is observed in neither $ZrCr_2H_x$ nor the hcp solid solutions, a partially (short-range) ordered structure may appear in $ZrCr_2H_x$ as it does in the hcp systems. The short-range order appears continuously with decreasing temperature, so no sharp phase transition is evident and no new Bragg peaks appear.

A change in the hydrogen structure affects the second moment because of its sensitivity to the relative positions of the hydrogen atoms. For a powdered sample, such as in the present work, the second moment is given by[10]

$$M_2=\tfrac{3}{5}\gamma^4\hbar^2 I(I+1)\sum_k r_{jk}^{-6}, \tag{9}$$

TABLE III. $T_{1\rho}^{-1}$ and T_1^{-1} maxima at each frequency for $x=0.2$ as well as the calculated values for the parameter $\mathfrak{R}$.

$(T_{1\rho}^{-1})_{\mathrm{MAX}}$ (s^{-1})	Frequency (kHz)	$(T_1^{-1})_{\mathrm{MAX}}$ (s^{-1})	Frequency (MHz)	$\mathfrak{R}_{\mathrm{expt}}$	$\mathfrak{R}_{\mathrm{dist}}$[a]
893	22.7	4.17	11.0	0.442	0.161
893	22.7	2.49	19.3	0.422	0.152
893	22.7	2.35	21.3	0.405	0.172
588	39.1	4.17	11.0	0.501	0.166
588	39.1	2.49	19.3	0.478	0.158
588	39.1	2.35	21.3	0.459	0.178

[a]Calculated from Gaussian distribution of activation energies; see Table I, second row.

TABLE IV. Second moments M_2 from fits to T_1^{-1} data and $T_{1\rho}^{-1}$ data, Van Vleck calculation, and measurement from magic echoes.

	$ZrCr_2H_{0.2}$	$ZrCr_2H_{0.5}$
M_2, T_1^{-1} fit (s^{-2})	0.6×10^9	1.7×10^9
M_2, $T_{1\rho}^{-1}$ fit (s^{-2})	0.8×10^9	1.7×10^9
M_2, Van Vleck (s^{-2})	1.11×10^9	2.67×10^9
M_2, magic echo (s^{-2})	1.4×10^9	2.3×10^9

where r_{jk} is the distance between hydrogen atoms j and k. Because of the r_{jk}^{-6} dependence, the second moment depends strongly on the average spacing between hydrogen atoms. Any change in the local structure resulting in a change in the average hydrogen spacing would be evident in the second moment.

We note that the possible variation of M_2 with structural changes is very large for a *dilute* system, such as $ZrCr_2H_x$ with $x=0.2$ (roughly 5% of the ''full loading''). At one extreme, a segregated or clustered system forms a fully hydrogen-dense structure. At the other extreme, the hydrogen atoms may remain maximally distant from each other by forming a superlattice. In between the two extremes is random occupation of the sites. For a hydrogen dilution factor Y,

$$Y \equiv \frac{x_{\text{actual}}}{x_{\text{fully loaded}}}; \tag{10}$$

the relative second moments of the clustered, randomly occupied, and maximally separated structures are 1, Y, and Y^2, for dipole interactions (R^{-3}). For $ZrCr_2H_x$ with $x=0.2$, the dilution factor[8] is ~ 0.05 ($x_{\text{fully loaded}} \sim 4$), so the three cases described above have dramatically different second moments. Thus, it is easy to envision local structural modifications that give rise to substantial changes in the second moment. We note that the local structural changes may also be responsible for the changes in apparent activation energy (see above and the temperature of the peak in Fig. 3).

We note that the Van Vleck calculated second moments are in reasonable accord with the low-temperature magic-echo data (Table IV). The calculations assumed random g-site occupation, except for a 2.1-Å exclusion distance. We emphasize that agreement between experiment and the second moment for an assumed structure *does not require* that the structure be correct—many structures have similar second moments. Indeed, we do not expect random occupation of g sites to be a good model at low temperatures where even weakly attractive or repulsive forces will be important.

Another possible explanation for the changing second moment is rapid localized motions between two asymmetric wells (Fig. 5). Rapid hopping between two sites would partially average the dipolar interaction, leading to a smaller effective second moment at higher temperatures. At lower temperatures, k_BT would become small in comparison to the asymmetry energy E_1 and the motion would be frozen out. Because the local motion is faster than the main diffusive motion, the freeze-out of the local motion cannot involve the barrier energy E_2 becoming too large compared to k_BT.

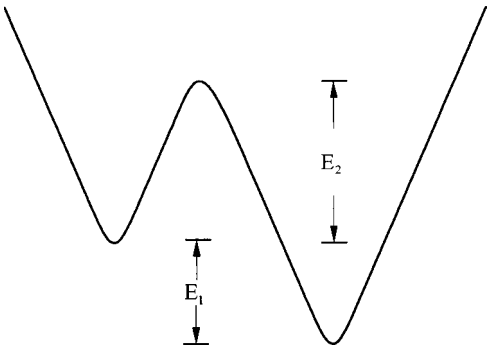

FIG. 5. Asymmetric potential well for a model of local hydrogen motions in $ZrCr_2H_x$. At low temperatures ($k_BT \ll E_1$), the local motions are frozen out. At higher temperatures, the effective second moment will be reduced by rapid motion between the two potential minima.

Rapid localized motions have been seen in the related $C15$-TaV_2H_x compound, as discussed in the Introduction.

IV. CONCLUSIONS

We have found that for $C15$-$ZrCr_2H_x$ (for $x=0.5$ and especially $x=0.2$) the observed spin-lattice relaxation rate in the rotating frame $T_{1\rho}^{-1}$ is much larger than expected from a model with a distribution of activation energies that describes the laboratory-frame spin-lattice relaxation rate T_1^{-1} at higher temperatures. To characterize this we have defined the dimensionless number $\mathfrak{R}$ that expresses the relative strength of the maximum rates $T_{1\rho}^{-1}$ and T_1^{-1}, corrected for the different measurement frequencies. For the $x=0.5$ sample, $\mathfrak{R}$ is nearly as large as expected from the simple BPP model and is larger than expected for the model used to fit T_1^{-1}. For the $x=0.2$ sample, $\mathfrak{R}$ is larger than expected for the BPP model and is nearly three times as large as expected for the model used to fit T_1^{-1}. Thus, there is strong evidence that the effective second moment of the dipolar interactions increases with decreasing temperature, especially for $x=0.2$. This is confirmed by direct measurement of M_2 at low temperatures using the magic-echo pulse sequence. The increase in second moment at lower temperatures is believed to be due to local ordering of the hydrogen, which causes the hydrogen to be closer on average as the temperature decreases. The effect may also be due to local hydrogen motion that partially averages the dipolar interaction leading to a smaller effective second moment at higher temperatures; at lower temperatures the local motion is presumed frozen out by the energetic asymmetry of the potential wells.

ACKNOWLEDGMENTS

We thank A. V. Skripov for providing the samples used in this study, as well as for numerous conversations about the data. We also appreciate conversations concerning these results with P. A. Fedders, G. Majer, R. G. Barnes, and A. F. McDowell. We gratefully acknowledge the support of the National Science Foundation through Grants Nos. DMR-9403667 and DMR-9705080.

[1] A. V. Skripov and M. Yu. Belyaev, J. Phys.: Condens. Matter **5**, 4767 (1993).
[2] A. V. Skripov, M. Yu. Belyaev, and A. P. Stepanov, Solid State Commun. **78**, 909 (1991).
[3] A. V. Skripov, M. Yu. Belyaev, S. V. Rychkova, and A. P. Stepanov, J. Phys.: Condens. Matter **1**, 2121 (1989).
[4] A. V. Skripov, J. C. Cook, C. Karmonik, and R. Hempelmann, J. Phys.: Condens. Matter **8**, L319 (1996).
[5] J.-J. Didisheim, K. Yvon, P. Fischer, and D. Shaltiel, J. Less-Common Met. **73**, 355 (1980).
[6] V. A. Somenkov and A. V. Irodova, J. Less-Common Met. **101**, 481 (1984).
[7] J. H. Wernick, in *Intermetallic Compounds*, edited by J. H. Westbrook (Wiley, New York, 1967).
[8] D. Fruchart, A. Rouault, C. B. Shoemaker, and D. P. Shoemaker, J. Less-Common Met. **73**, 363 (1980).
[9] J. H. Van Vleck, Phys. Rev. **74**, 1168 (1948).
[10] A. Abragam, *Principles of Nuclear Magnetism* (Oxford, London, 1961).
[11] W. Renz, G. Majer, A. V. Skripov, and A. Seeger, J. Phys.: Condens. Matter **6**, 6367 (1994).
[12] E. Fukushima and S. B. W. Roeder, *Experimental Pulse NMR* (Addison-Wesley, Reading, MA, 1981).
[13] R. C. Bowman and W.-K. Rhim, J. Magn. Reson. **49**, 93 (1982).
[14] J. Jeener and P. Broekaert, Phys. Rev. **157**, 232 (1967).
[15] C. P. Slichter, *Principles of Magnetic Resonance* (Springer-Verlag, Berlin, 1990).
[16] N. Bloembergen, E. M. Purcell, and R. V. Pound, Phys. Rev. **73**, 679 (1948).
[17] C. A. Sholl, J. Phys. C **7**, 3378 (1974).
[18] D. C. Look and I. J. Lowe, J. Chem. Phys. **44**, 2995 (1966).
[19] O. Blaschko, J. Pleschiutschnig, L. Pintschovius, J. P. Burger, J. N. Daou, and P. Vajda, Phys. Rev. B **40**, 907 (1989).
[20] M. W. McKergow, D. K. Ross, J. E. Bonnet, I. S. Anderson, and O. Schaerpf, J. Phys. C **20**, 1909 (1987).
[21] O. Blaschko, G. Krexner, J. N. Daou, and P. Vajda, Phys. Rev. Lett. **55**, 2876 (1985).